Current Research in Food Science 8 (2024) 100702

Contents lists available at ScienceDirect

Current Research in Food Science

journal homepage: www.sciencedirect.com/journal/current-research-in-food-science

Phytosterol organic acid esters: Characterization, anti-inflammatory properties and a delivery strategy to improve mitochondrial function

Xinyue Zou [a,1], Ting Xu [b,1], Tian Zhao [b], Jing Xia [b], Feifan Zhu [c], Yu Hou [d], Baiyi Lu [b], Yunfei Zhang [a,**], Xuan Yang [b,*]

[a] Department of Chemistry, China Agricultural University, Beijing, 100193, China
[b] College of Biosystems Engineering and Food Science, Key Laboratory for Quality Evaluation and Health Benefit of Agro-Products, Ministry of Agriculture and Rural Affair, Interdisciplinary Research Center on Optical Agricultural and Food Engineering, Zhejiang University, No. 866 Yuhangtang Road, Hangzhou, Zhejiang, 310058, China
[c] Zhejiang University School of Medicine, Hangzhou, Zhejiang, 310058, China
[d] Liangzhu Laboratory, Zhejiang University, No. 1369 West Wenyi Road, Hangzhou, 311121, China

ARTICLE INFO

Handling Editor: Dr. Yeonhwa Park

Keywords:
Phytosterol esters
Stigmasterols
Phenolic acids
Steglich reaction
Anti-inflammatory
Mitochondrial delivery strategy

ABSTRACT

Phytosterol organic acid esters are important food resources and the components of biomembrane structure. Due to the lack of extraction and synthesis techniques, more research has been focused on phytosterols, and the research on phytosterol acid esters have encountered a bottleneck, but phytosterol acid esters confer substantial benefits to human health. In this study, stigmasteryl vanillate (VAN), stigmasteryl protocatechuate (PRO) and stigmasteryl sinapate (SIN) were prepared through the Steglich reaction. The processes are promotable and the products reach up to 95% purity. In addition, their stability was evaluated by differential scanning calorimetry and thermogravimetric analysis. HPLC analysis revealed an enhancement in water solubility after esterification with phenolic acid. In an *in vitro* digestion model, the bioaccessibility of stigmasteryl phenolates was significantly higher than that of stigmasterols (STIs). Regarding the anti-inflammatory properties, VAN, PRO, and SIN exhibit superior effects against TNF-α induced pro-inflammatory responses compared to STI. All stigmasteryl phenolates supplementation increased the ATP production, the basal, and maximal oxygen consumption rate in mitochondrial stress test. Overall, we present a synthesis method for stigmasteryl phenolates. It will contribute to the development and research of phytosterol acid ester analysis, functions and utilization in food. Moreover, the nutrient-stigmasterol hybrids tactic we have constructed is practical and can become a targeted mitochondrial delivery strategy with enhanced anti-inflammatory effects.

1. Introduction

Phytosterols are important micronutrients, which cannot be synthesized by the human body, often added to orange juice, low-fat yogurt, chocolate and milk as dietary supplements to ensure human health (Andreasen et al., 2001; Zhang et al., 2022). Phytosterol esters are the forms of phytosterols present in natural plants, accounting for approximately 30–80% of the total sterol content, and are mostly distributed in grain and plant seeds, such as soybean, olive, cotton seed, lotus seed, coconut, safflower, and peanut oil (Broughton and Beaudoin, 2021; Cercaci et al., 2003; Flakelar et al., 2017).

Due to its easier absorption and utilization by the human body, phytosterol esters has received widespread attention in the food industry since 1995 (Clifton et al., 2004). In recent years, the research on phytosterol organic acid esters has also received increasing attention (Liu et al., 2021; Zheng et al., 2013). Scholars have attempted to prepare

Abbreviations: STI, stigmasterol; VAN, stigmasteryl vanillate; PRO, stigmasteryl protocatechuate; SIN, stigmasteryl sinapate; DMAP, 4-dimethylamino pyridine; DIC, *N,N′*-diisopropylcarbodiimide; DCC, dicyclohexylcarbodiimide; HPLC, high performance liquid chromatography; HRMS, high resolution mass spectrum; FTIR, Fourier transform infrared spectroscopy; NMR, nuclear magnetic resonance; TGA, thermogravimetric analysis; DSC, differential scanning calorimetry; OCR, oxygen consumption rate; SSF, simulated salivary fluid; SGF, simulated gastric fluid; SIF, simulated intestinal fluid.

* Corresponding author.
** Corresponding author.
E-mail addresses: zyfeichem@cau.edu.cn (Y. Zhang), yangxuan218@zju.edu.cn (X. Yang).
[1] These authors contributed equally to this work.

https://doi.org/10.1016/j.crfs.2024.100702
Received 12 November 2023; Received in revised form 16 January 2024; Accepted 15 February 2024
Available online 26 February 2024

them using enzymatic methods (Schär et al., 2017), however, there are still certain bottlenecks in preparation efficiency and product purity. Stigmasterol (STI) is a steroid with high nutritional value that impacts antioxidation, inflammation, cholesterol homeostasis, stress response, and mitochondrial function (Jie et al., 2022). It demonstrates striking effects on reducing intestinal cholesterol absorption and preventing cardiovascular disease, cerebrovascular disease and age-related cognitive decline (Rui et al., 2017). However, the limited water solubility of phytosterols such as STI restricts their application (He et al., 2018; Sakamoto et al., 2013; Witkowska et al., 2022). Still, as a cholesterol analog, STI acts as an effective metabolic regulator (Di Trani et al., 2022).

Phenolic acids are organic acids containing phenolic rings, derived from plant directly, degradation of flavonoids in plants, and gut microbial flavonoid metabolism (Osborn et al., 2021). Phenolic acids have extensive applications. As naturally abundant phenolic acids, vanillic acid, protocatechuic acid, and sinapic acid have been comprehensively studied. These three phenolic acids are naturally enriched in grain, fruits and vegetables and provide cytoprotection (Andreasen et al., 2001; Dhar et al., 2007; Juurlink et al., 2014; Tan and Shahidi, 2013). In particular, they work synergistically with phytosterols to inhibit lipid peroxidation, regulate the lipids profile, endoplasmic reticulum stress response, and mitochondrial function in cells (Ashokkumar and Vinothiya, 2023; He et al., 2018; Mohan et al., 2023). They also have anti-inflammatory, cardioprotective, and neuroprotective effects (Li et al., 2023; Semaming et al., 2014; Winter et al., 2017; Yalameha et al., 2023). Further, due to its molecular weight and brain barrier permeability, these dietary phenolic acids are considered to have peroxynitrite scavenging activity against diseases involving peroxynitrite (Niwa et al., 1999), and have cerebral benefits (Karakida et al., 2007). Therefore, natural products are considered to be added in food systems, such as oil industry, and the changes in lipid composition are very closely related to inflammation (Andersen, 2022). However, the solubility of sterols is limited, the independent addition of phenolic acids will lead to flocculent precipitation, and the system is not stable, so it is urgent to apply the derivatization of sterols and phenolic acids (Amaral et al., 2003; Tai et al., 2018).

Owing to the biological activity of molecules containing stigmasterol or phenolic acid in many areas of chemistry, we aimed to synthesize sterol ester by incorporating phenolic acid into stigmasterol. This improves the physical and chemical properties of compounds, such as water solubility. More importantly, phenolic acids regulate the molecular conformation of stigmasterol and enhance its biological potency. Motivated by the potential benefits, the objective of this research was to design and prepare three novel compounds: stigmasteryl vanillate, stigmasteryl protocatechuate, and stigmasteryl sinapate, which were synthesized by screening condensation reagents, catalysts, solvents, and reaction times. Direct condensation with DCC and DMAP produced stigmasteryl vanillate, stigmasteryl protocatechuate, while stigmasteryl sinapate were prepared through a protection, esterification, and potassium carbonate deprotection process. The reagents used in the process are non-toxic and required in low amounts, making the synthesis safer. NMR spectra revealed the prepared sterol esters achieved high purities up to 95%. We investigated the physical properties and bioaccessibility of these new sterol-phenolic acid conjugates in order to expand their applications from mitochondrial function, anti-inflammatory and resource utilization perspectives.

2. Materials and methods

2.1. Materials

Stigmasterol, triethylamine, acetic anhydride, vanillic acid, protocatechuic acid and sinapic acid were purchased from Energy Chemical (Anhui, China). 4-(dimethylamino) pyridine (DMAP) was purchased from Alfa Aesar (Beijing, China). Dicyclohexylcarbodiimide (DCC) was purchased from Heowns (Tianjin, China). Potassium carbonate (K_2CO_3) was purchased from Macklin (Shanghai, China). All other common reagents were of analytical grade. Flash chromatography was performed using silica gel (300–400 mesh) from Qingdao Ocean Chemical.

2.2. Preparation of esterification of stigmasterol

The preparation strategy of VAN, PRO and SIN were shown in Fig. 1. Initially, synthesizing the three novel compounds is quite challenging. To optimize the synthesis and achieve high yields, extensive efforts were undertaken to methodically evaluate various reaction parameters, including: types of reagents, reagent dosages, catalysts, reaction temperatures, solvent selections and reaction time (Supplementary Tables S1–S3).

As shown in Supplementary Table S1, we first evaluated a series of commonly used condensation agents were evaluated. No product was generated until DCC (dicyclohexylcarbodiimide) and DIC (*N*, *N*′-diisopropylcarbodiimide) was employed (entries 1–3). Then, inspired by previous reports (Fu et al., 2014; Jia et al., 2019; Winkler-Moser et al., 2015), we reduced the starting reaction temperature to 0 °C and increased the yield (entries 4–5). We also screened other solvents (entries 6–8) and different reactant ratios (entry 7, 9). Finally, the optimized condition was obtained with higher yields (entry 9). The specific preparation steps are shown in Supporting Information.

Based on the conditions that synthesized stigmasteryl vanillates, we chose to use DCC as a condensation agent for the synthesis of stigmasteryl protocatechuate. As shown in Supplementary Table S2, various solvents were screened based on reactant solubility while no satisfied yield was obtained (entries 1–4). Then we increased the DCC equivalent and reduced the DMAP equivalent, obtaining a 36% yield (entry 5). The absence of DMAP decreased the yield slightly (entry 6). Furthermore, a lower yield was obtained when the reaction proceeded directly at room temperature (entry 7).

The phenolic hydroxyl group of sinapic acid readily underwent esterification with the carboxyl group, so direct esterification did not produce stigmasteryl sinapates. Therefore, we had to protect the hydroxyl group of the phenolic acid first. The protected phenol hydroxyl group was deprotected after esterification. As shown in Supplementary Table S3, Tol/THF (1:1) was later examined to reach higher yield, likely due to the solubility of the sinnapic acid (entries 1–4). Then, adjusting the equivalents of DCC and DMAP (entries 5–7) yielded the best result of 73%.

2.2.1. Synthesis of stigmasteryl vanillate (VAN)

The specific preparation steps are as follows: Vanillic acid (126.1 mg, 0.75 mmol) and stigmasterol (206.3 mg, 0.5 mmol) were dissolved in 15 mL of DCM/THF (1:1) solution at 0 °C. Add the DCC (154.7 mg, 0.75 mmol) and stir for 15 min. After the complete dissolution of reactants, DMAP (3.1 mg, 0.025 mmol) was added to the solution. The reaction mixture was stirred at room temperature overnight, then filtered using a funnel with G4 sintered disc to remove white precipitate. The filtrate was extracted by EtOAc, washed with saturated aqueous NH_4Cl and brine, dried over anhydrous Na_2SO_4, filtered, and the solvent was evaporated under vacuum. The crude product was purified by column chromatography (eluant: petroleum ether/ethyl acetate, 15:1. V/V) to afford the product (53.4 mg, 19%) as a white solid.

2.2.2. Synthesis of stigmasteryl protocatechuate (PRO)

The specific preparation steps are as follows: To a solution of protocatechuic acid (154.1 mg, 1 mmol) and stigmasterol (412.7 mg, 1 mmol) in 15 mL of DCM/THF (1:1) at 0 °C was added DCC (453.9 mg, 2.1 mmol) in solution and stir for 15 min. After the complete dissolution of reactants, DMAP (3.1 mg, 0.025 mmol) was added to the solution. The reaction mixture was stirred at room temperature overnight, then filtered using a funnel to remove white precipitate. The filtrate was extracted by EtOAc, washed with saturated aqueous NH_4Cl and brine,

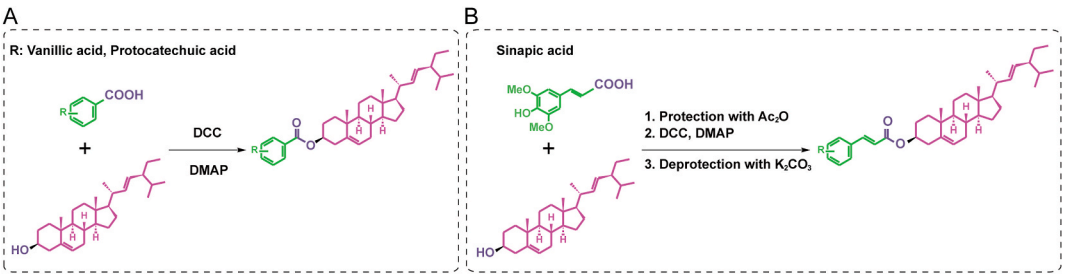

Fig. 1. Preparation of stigmasteryl phenolates. (A) Synthesis of esterification of stigmasteryl benzoate. Stigmasterol reacted with phenolic acid in the presence of dicyclohexylcarbodiimide (DCC) and 4-dimethylamino pyridine (DMAP); (B) synthesis of ssterification of stigmasteryl styrylate. Step 1, sinapic acid was protected with acetic anhydride (Ac_2O); step 2, stigmasterol reacted with protected sinapic acid in the presence of DCC and DMAP; step 3, deprotection with K_2CO_3.

dried over anhydrous Na_2SO_4, filtered, and the solvent was evaporated under vacuum. The crude product was purified by column chromatography (eluant: petroleum ether/ethyl acetate, 20:1. V/V) to afford the product (197.4 mg, 36%) as a pale-yellow solid.

2.2.3. Synthesis of stigmasteryl sinapate (SIN)

The phenolic hydroxyl group of sinapic acid readily underwent esterification with the carboxyl group, so direct esterification did not produce stigmasteryl sinapates. Therefore, we had to protect the hydroxyl group of the phenolic acid first. The protected phenol hydroxyl group was deprotected after esterification.

For synthesis of protected sinapic acid: triethylamine (0.12 mL, 1.5 mmol) was added to a solution of sinapic acid (154.1 mg, 1 mmol) in 5 mL of DCM at 0 °C followed by dropwise addition of acetic anhydride (0.15 mL, 1.5 mmol). Then DMAP (193.2 mg, 0.01 mmol) was added. The mixture was stirred at 0 °C for 10 min, warmed to room temperature slowly and stirred for 4 h at room temperature. Then 2 M HCl was slowly added at 0 °C. The resulting solution was washed with saturated aqueous NH_4Cl and brine. The organic layer was dried over anhydrous Na_2SO_4, filtered and concentrated under reduced pressure to dryness to give the product (202.2 mg, 76%) as a yellow solid.

For synthesis of protected stigmasteryl sinapate: To a solution of protected sinapic acid (224.2 mg, 1 mmol) and stigmasterol (412.7 mg, 1 mmol) in 10 mL of Tol/THF (1:1) solution at 0 °C was added DCC (453.9 mg, 2.1 mmol) in solution and stir for 15 min. After the complete dissolution of reactants, DMAP (3.1 mg, 0.025 mmol) was added to the solution. The reaction mixture was stirred at room temperature overnight, then filtered using a funnel to remove white precipitate. The filtrate was extracted by EtOAc, washed with saturated aqueous NH_4Cl and brine, dried over anhydrous Na_2SO_4, filtered, and the solvent was evaporated under vacuum. Purification over a silica gel chromatography eluted with petroleum ether/ethyl acetate (15:1. V/V) gave the product (482.5 mg, 73%) as a white solid.

For synthesis of stigmasteryl sinapate: To a stirred solution of above product (660.1 mg, 1.0 mmol) in 5 mL of chloroform/methanol (2:1) was slowly added K_2CO_3 (27.6 mg, 0.2 mmol). Then the mixture was refluxed for 6 h. After cooling down to room temperature, solvent was removed from the reaction mixture using rotary evaporator. The crude product was extracted with EtOAc and washed with saturated aqueous NH4Cl and brine, dried over anhydrous Na_2SO_4, filtered, and the solvent was evaporated under vacuum. The crude product was purified by silica gel column chromatography eluted with petroleum ether/ethyl acetate (15:1. V/V) to deliver the product (464.2 mg, 75%) as a white solid.

2.3. Characterization of products by HRMS, FTIR and NMR

2.3.1. HRMS analysis

High-resolution MS was conducted on a Bruker Daltonics Flex-Analysis spectrometer (Bao et al., 2022).

2.3.2. FTIR analysis

The FTIR spectra were recorded using Nicolet IS10 FTIR spectrophotometer (Thermo, USA). The scan times are 16 and the resolution is 4 cm^{-1} with the spectral scanning scope for 400–4000 cm^{-1}.

2.3.3. NMR analysis

NMR spectra of pure VAN, PRO and SIN were recorded on Bruker AVANCE 500 and Bruker AVANCE 600. Method was the previous reports (Yu et al., 2023). Chemical shifts for protons are reported in parts per million downfield from tetramethylsilane and are referenced to residual protium in the NMR solvent ($CHCl_3$ = δ 7.262). Chemical shifts for carbon are reported in parts per million downfield from tetramethylsilane and are referenced to the carbon resonances of the solvent ($CDCl_3$ = δ 77.0). Data are represented as follows: chemical shift, multiplicity (s = singlet, d = doublet, t = triplet, q = quartet, m = multiplet), coupling constants in Hertz (Hz), integration.

2.4. HPLC analysis

The HPLC analysis was performed using a Shimadzu LC-20AT equipped with an SPD-20A UV-detector (Yu et al., 2023). An Agilent ZORBAX SB-C18 (250 × 4.6 mm) column was employed. The parameters of Shimadzu HPLC system were listed as follows: wavelength: 270 nm (VAN, PRO and SIN) and 220 nm (STI), oven temperature: 30 °C, solvent: methanol with 0.1% formic acid, flow: 1.0 mL/min, injection: 10 μL.

2.5. DSC analysis

The melting and crystallization characteristics of STI and three stigmasteryl phenolates were determined by DSC. The samples were dried under vacuum at 50 °C for 0.5 h. The 3.0–8.0 mg samples were then transferred to a crucible and thermal analysis was performed using a differential scanning calorimeter. All the samples were held for 5 min at 25 °C, and then heated to 300 °C at a rate of 20 °C/min, cooled from 300 °C to 25 °C at a rate of 20 °C/min.

2.6. TGA analysis

STI and three types of stigmasteryl phenolates were weighed between 8.0 and 12.5 mg, and performed in a SDT-Q600 simultaneous TGA/DSC series thermal analysis system (TA, USA). The dried samples were heated at 20 °C/min up to 515 °C under inert atmosphere of N_2 in a flow rate of 120 mL/min.

2.7. Solubility test

0.1 g of STI or stigmasteryl phenolates were put into 10 mL of deionized water. After ultrasonic dissolving for 8 h, the samples were placed at 25 °C in a constant temperature water bath for 1 h. The upper phase (50 μL) was pipetted and diluted in 10 mL of methanol. The water

solubility was determined by comparing the chromatographic peak area of the sample solution with that of the standard sample solution.

2.8. In vitro digestion

In vitro digestion was performed according to the INFOGEST 2.0 method reported by Brodkorb (Brodkorb et al., 2019). Briefly, 5 mg of samples and 5 mL of deionized water were transferred to a volumetric flask and 5 mL of oral digestive fluid, containing simulated salivary fluid and $CaCl_2$. The solution was incubated at 37 °C in a magnetic stirrer for 2 h. At the end of the oral digestion, transfer 5 mL of the oral digest mixture to another volumetric flask and 5 mL of gastric digestive fluid containing simulated gastric fluid, pepsin, HCl and $CaCl_2$. Then, the solution was incubated at 37 °C in a magnetic stirrer for 2 h. Next, transfer 5 mL of the gastric digestive products to another volumetric flask and 5 mL of intestinal digestive fluid containing simulated intestinal fluid, trypsin mixture, bile, NaOH and $CaCl_2$. And the solution was incubated at 37 °C in a magnetic stirrer for another 2 h. After completion of the intestinal digestion, the reaction was terminated by the addition of NaOH solution to pH 7.0. The final mixture was divided equally into two parts. One part was centrifuged at 10,000 rpm for 15 min at 4 °C, and the upper layer was used as the supernatant; the other part was used as the digestion solution without further processing.

All samples were analyzed by HPLC. Bioaccessibility (B) of samples in a simulated digestive system was calculated using the following equation:

$$B = \frac{A_s}{A_d} \times 100\%$$

where A_s is the peak areas of supernatant, A_d is the peak areas of digestion solution.

2.9. Cell culture and treatment

The renal proximal tubular cell, human kidney 2 cells (HK-2) were purchased from the national experimental cell resource sharing platform at Peking Union Medical College. The human embryonic kidney cells (HEK-293), murine colon carcinoma cells (MC-38) and HeLa cells were gifted from Dr Hou's Lab. Cells were cultured according to the previous study (Yang et al., 2019). The pro-inflammatory cytokines, 200 ng/mL tumor necrosis factor alpha (TNF-a) (Solarbio, PRC) were to induce acute renal inflammatory response in HK-2 cells (Lee et al., 2017). The CCK-8 kit (Solarbio, PRC) were used to the assessment of cell viability.

2.10. Measurement of oxygen consumption rate

The measurement of oxygen consumption rate (OCR) was measured using a Seahorse XF96 Extracellular Flux Analyser (Seahorse Bioscience, Agilent Technologies, Santa Clara, CA), and Seahorse XF Cell Mito Stress Test Kit (103,015–100; Seahorse Bioscience). The OCR and ATP production detection of HK-2 cells was according to the protocol (Gu et al., 2020). The OCR changes of HK-2 cells were measured after 24h treatment of 20 μM STI, and three stigmasteryl phenolates.

3. Results and discussions

3.1. Structural analysis of products

The preparation strategy of VAN, PRO and SIN were shown in Fig. 1, and all of the purified components were analyzed by HRMS, FTIR, and NMR and the results were listed as follow:

For VAN, HRMS (ESI) m/z calcd for C37H55O4 $[M + H]^+$: 563.4094; found 563.4095. FTIR (ν, cm−1): 3521, 2936, 2867, 1707, 1593, 1514, 1463, 1434, 1368, 1289, 1222, 1104, 1028.^{1}H NMR (500 MHz, Chloroform-d) δ 7.64 (dd, J = 8.3, 1.9 Hz, 1H), 7.54 (d, J = 1.9 Hz, 1H), 6.93 (d, J = 8.3 Hz, 1H), 6.00 (s, 1H), 5.41 (dd, J = 5.0, 2.0 Hz, 1H), 5.16 (dd, J = 15.1, 8.7 Hz, 1H), 5.02 (dd, J = 15.1, 8.7 Hz, 1H), 4.83 (dtd, J = 16.3, 8.5, 4.5 Hz, 1H), 3.95 (s, 3H), 2.45 (d, J = 8.0 Hz, 2H), 2.08–1.88 (m, 5H), 1.77–1.67 (m, 2H), 1.60–1.35 (m, 9H), 1.29–1.13 (m, 6H), 1.09–0.98 (m, 9H), 0.87–0.77 (m, 9H), 0.71 (s, 3H). ^{13}C NMR (126 MHz, Chloroform-d) δ 165.8, 149.8, 146.1, 139.7, 138.3, 129.3, 124.1, 123.0, 122.7, 113.9, 111.7, 74.4, 56.8, 56.1, 55.9, 51.2, 50.1, 42.2, 40.5, 39.6, 38.3, 37.1, 36.7, 31.9, 31.9, 28.9, 27.9, 25.4, 24.4, 21.2, 21.1, 21.0, 19.4, 19.0, 12.2, 12.0.

For PRO, HRMS (ESI) m/z calcd for $C_{36}H_{53}O_4$ $[M + H]^+$: 549.3938; found 549.3934. FTIR (ν, cm^{-1}): 3467, 3366, 2953, 2925, 2852, 1682, 1607, 1442, 1291, 1234, 1166, 1102.^{1}H NMR (600 MHz, Chloroform-d) δ 7.60–7.56 (m, 2H), 6.90 (d, J = 7.9 Hz, 1H), 5.78 (s, 1H), 5.56 (s, 1H), 5.41 (s, 1H), 5.19–5.12 (m, 1H), 5.05–4.98 (m, 1H), 4.83–4.77 (m, 1H), 2.44 (d, J = 8.2 Hz, 2H), 2.07–1.88 (m, 6H), 1.74–1.66 (m, 2H), 1.55–1.41 (m, 6H), 1.32–1.12 (m, 11H), 1.08–1.00 (m, 7H), 0.87–0.78 (m, 9H), 0.70 (s, 3H). ^{13}C NMR (126 MHz, Chloroform-d) δ 165.8, 148.3, 142.8, 139.7, 138.3, 130.0, 123.8, 123.5, 122.8, 117.2, 114.8, 75.0, 56.8, 55.9, 51.2, 50.1, 42.2, 40.5, 39.6, 38.2, 37.0, 36.7, 31.9, 31.9, 29.8, 28.9, 27.9, 25.4, 24.8, 24.4, 21.2, 21.1, 21.0, 19.4, 19.0, 12.2, 12.0.

For SIN, HRMS (ESI) m/z calcd for $C_{40}H_{58}KO_5$ $[M + K]^+$: 657.3916; found 657.3920. FTIR (ν/cm^{-1}): 3413, 2939, 2866, 1700, 1636, 1595, 1517, 1459, 1278, 1175, 1114, 1019, 971, 826, 725.^{1}H NMR (500 MHz, Chloroform-d) δ 7.58 (d, J = 15.8 Hz, 1H), 6.77 (s, 2H), 6.29 (d, J = 15.9 Hz, 1H), 5.77 (s, 1H), 5.40 (d, J = 5.0 Hz, 1H), 5.15 (dd, J = 15.2, 8.6 Hz, 1H), 5.01 (dd, J = 15.2, 8.5 Hz, 1H), 4.80–4.69 (m, 1H), 3.91 (s, 6H), 2.40 (s, 2H), 2.09–1.85 (m, 5H), 1.76–1.38 (m, 12H), 1.34–0.93 (m, 18H), 0.90–0.76 (m, 10H), 0.70 (s, 3H). ^{13}C NMR (126 MHz, Chloroform-d) δ 166.5, 147.2, 144.7, 139.7, 138.3, 137.0, 129.3, 126.0, 122.7, 116.5, 105.0, 73.9, 56.8, 56.3, 55.9, 51.2, 50.0, 42.2, 40.5, 39.6, 38.3, 37.0, 36.6, 31.9, 28.9, 27.9, 25.4, 24.3, 21.2, 21.1, 21.0, 19.3, 19.0, 12.2, 12.0.

Theoretically, the relative molecular mass of VAN was 562.4022, PRO was 548.3866, and SIN was 618.4284. Thus, the protonated molecular ion $[M+H]^+$ at M/z 563.4095 for VAN, the protonated molecular ion $[M+H]^+$ at M/z 549.3934 for PRO and the potassium adduct molecular ion $[M+K]^+$ at M/z 657.3920 for SIN were observed under positive-ion mode, respectively.

The IR spectra of STI, VAN, PRO and SIN are shown in Fig. 2, which could provide evidence that the synthesized products were stigmasteryl esters. Compared with STI, a sharp absorption peak of C=O of phenolate appeared (1707 cm^{-1} for VAN, 1682 cm^{-1} for PRO and 1700 cm^{-1} for SIN), several absorption peak of phenyl group (1593 cm^{-1} and 1514 cm^{-1} for VAN, 1607 cm^{-1} for PRO, 1595 cm^{-1} and 1517 cm^{-1} for SIN) and an absorption peak of C–O–C appeared (1222 cm^{-1} for VAN, 1234 cm^{-1} for PRO and 1175 cm^{-1} for SIN) prove the existence of these phenolate groups. And a broad band around 3300-3500 cm^{-1} represents the remaining hydroxyl group in stigmasteryl phenolates.

The structures of stigmasteryl phenolates were further confirmed by ^{1}H NMR and ^{13}C NMR and NMR spectra of VAN, PRO and SIN were displayed in the **Supplementary data**, respectively. The proton peaks at δ 7.64 (dd), 7.54 (d), 6.93 (d), 6.00 and 3.95 ppm indicated that VAN was successfully produced. Similarly, the chemical shift of PRO at δ 7.60–7.56 and 6.90 (d) proved that STI was conjugated with protocatechuic acid; the peak at δ 7.58 (d), 6.77, 6.29 (d), 5.77 and 3.91 represented the formation of SIN. ^{13}C NMR peak at 165.8, 165.8, 166.5 ppm indicated the formed C=O bond in VAN, PRO and SIN, respectively.

3.2. Thermal analysis

The melting and crystallization properties of pure components are depicted by the DSC thermograms in Fig. 3. VAN exhibited two endothermic peaks at 118.6 °C (endothermic enthalpy ΔH = 30.82 J/g) and 259.6 °C (ΔH = 25.17 J/g) in the melting curve, likely representing the melting of polycrystals with lower and higher melting points. Between

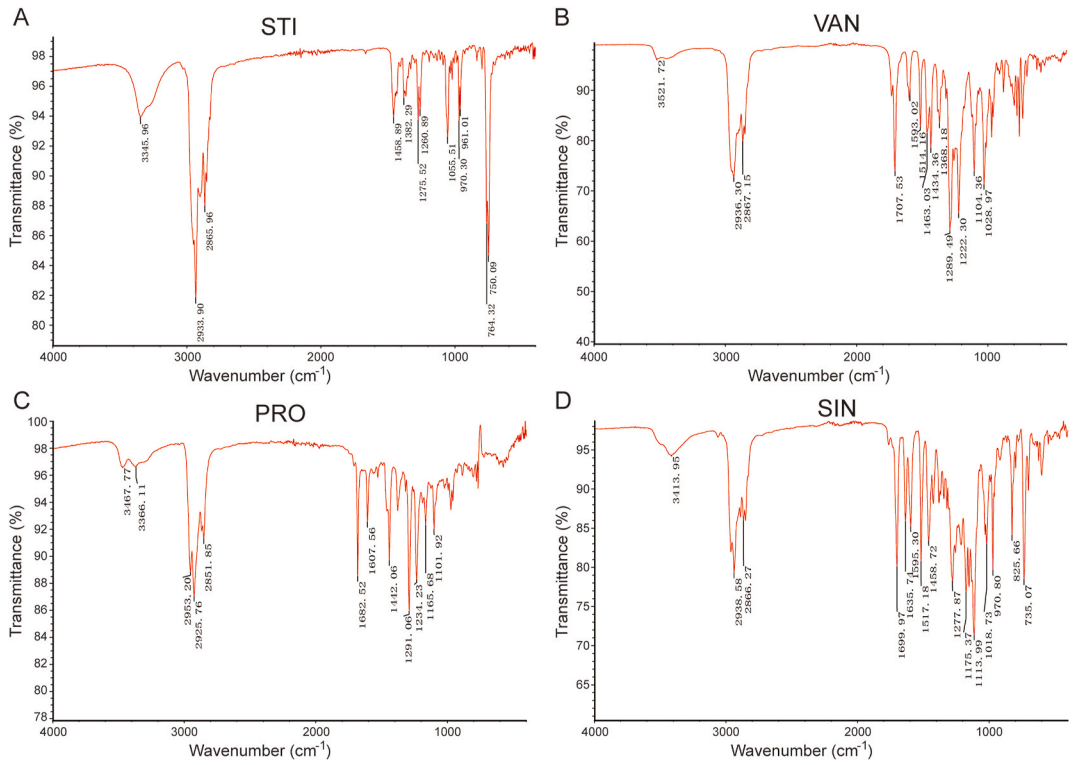

Fig. 2. FT-IR spectra of (A) stigmasterol (STI); (B) stigmasteryl vanillate (VAN); (C) stigmasteryl protocatechuate (PRO); (D) stigmasteryl sinapate (SIN).

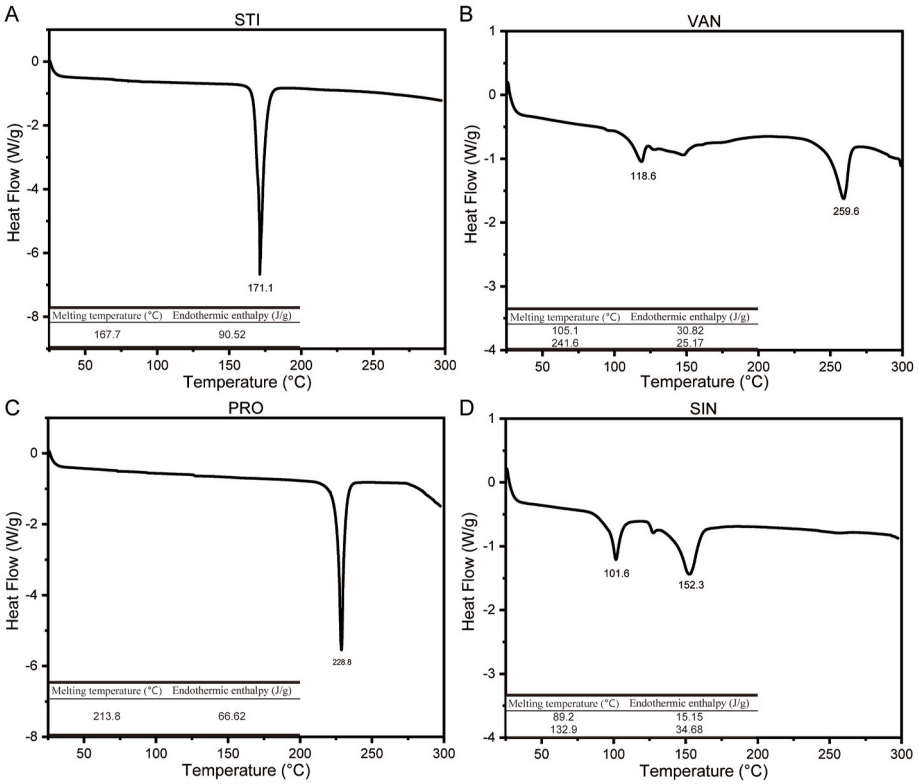

Fig. 3. DSC curves for (A) stigmasterol (STI); (B) stigmasteryl vanillate (VAN); (C) stigmasteryl protocatechuate (PRO); (D) stigmasteryl sinapate (SIN).

the two melting peaks was a small exothermic peak at 152.8 °C, respectively. Similarly, SIN showed two endothermic peaks at 101.6 °C (ΔH = 15.15 J/g) and 152.3 °C (ΔH = 34.68 J/g), which might be attributed to the melt mediated transformation of polymorph. Interestingly, PRO exhibited one endothermic peak at 228.8 °C (ΔH = 66.62 J/g), probably indicating PRO's melting peak. STI has one endothermic peak at 171.1 °C (ΔH = 90.52 J/g).

Among the three synthetic substances, PRO and the stable crystalline

form of VAN had the melting point at 213.8 °C and 241.6 °C, respectively, higher than STI (167.7 °C). While the stable crystalline form of SIN had a lower melting point of 132.9 °C than STI (167.7 °C).

3.3. Thermogravimetric analysis

The thermogravimetric curve of STI, VAN, PRO and SIN were shown in Fig. 4. The initial decomposition temperature of STI was around 250 °C. The temperature at 98.1% mass loss was 385.3 °C, and the char yield at 505.7 °C was 1.9%. For VAN, the temperature at 3.9 % mass loss was 200.0 °C and the initial decomposition occurred around 260.0 °C. The temperature at 75.4% mass loss was 420.0 °C, and the char yield at 506.3 °C was 14.8%. PRO initially decomposed around 200.0 °C. The temperature at 96.9% mass loss was 504.7 °C, and the char yield at 505.8 °C was 3.0%. For SIN, the temperature at 3.4% mass loss was 150.0 °C and the initial decomposition was around 280.0 °C. The temperature at 75.4% mass loss was 503.6 °C, and the char yield at 506.3 °C was 8.7%. In this dimension, STI, VAN, PRO and SIN had maximum mass loss rates at 380.9 °C, 364.0 °C, 377.1 °C and 377.8 °C, respectively.

3.4. Solubility assay analysis

Consistent with phytosterols, stigmasterols have a hydrophobic cyclopentane polyhydrophenanthrene structure, resulting in STI's low water solubility. We predicted that the introduction of phenolic acids containing hydrophilic phenol-OH group by esterification could improve its water solubility. As shown in Fig. 5A, the water solubilities of STI, VAN, PRO and SIN were 0.03, 0.09, 4.73 and 1.49 mg/mL respectively. The figure demonstrated that the introduction of phenolic hydroxyl groups improved STI's water solubility. PRO's solubility remarkably increased to 4.73 mg/mL due to two hydrophilic hydroxyl groups on its benzene ring, which also increased polarity. And the benzene ring of the SIN carries two methoxy and one hydroxyl groups, which also increases the polarity of the molecule. That is why SIN's solubility is increased to 1.49 mg/mL. Although VAN has a hydroxyl group, the presence of the ortho-methoxy and para-ester groups results in a balance of molecular polarity, leading to a slight change in its water solubility. The solubility data obtained in this study may provide potential application in food slike juice, tea, and emulsions.

3.5. In vitro bio-accessibility of stigmasteryl phenolates

To assess the endpoint products resulting from oral, gastric, intestinal digestion and the release of stigmasteryl phenolates from the potential food matrix, the bioaccessibility analysis was completed according to a widely recommended method (Brodkorb et al., 2019). At digestion's end, as shown in Fig. 5B, the bioaccessibilities of VAN, PRO and SIN were 93.2%, 91.2% and 94.1%, respectively, higher than STI's 83.4%. Higher bioaccessibility means easier digestion and transport in the stomach and intestines. Although this paper did not carry out *in vivo* experimental validation in mice, based on our *in vitro* observations, stigmasteryl phenolates were clearly more readily digested and released by artificial digestive fluid than STI, this would be very helpful as a potential replacement for STI in foods such as fats, chocolate, energy bars, etc.

3.6. Anti-inflammatory activity

The recommended dietary intervention for sterols in mice is 0.2 g/kg bw (Wang et al., 2021a). Under this model for 14 weeks, the concentration of stigmasterol in serum was 5 μg/mL (12 μM), and 6 μg/mL (15 μM) in the liver (Wang et al., 2021b). Thus, 0–100 μM concentration of phytosterol acid esters were considered to study the role of cell viability in HK-2 cells (Fig. 6A). Compared with STI, the VAN, PRO and SIN did not show significant differences of cell viability *in vitro*. Multiple cell lines were also considered to analyze the relationship between STI and cell viability (Fig. 6B). When the concentration of stigmasterol was below 20 μM, it has little effect on the viability of different cell lines. When the concentration of stigmasterol was above 50 μM, higher than that of dietary exposure dose, there was a significant difference in its

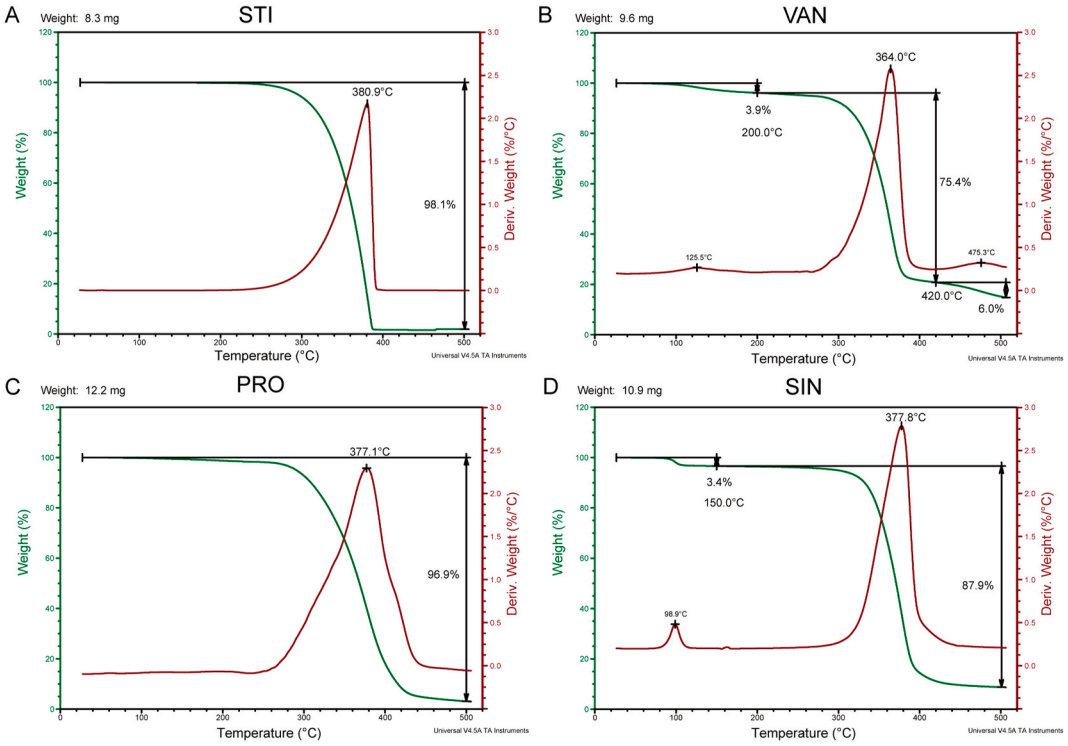

Fig. 4. Experimental mass fraction of stigmasterol (STI), stigmasteryl vanillate (VAN), stigmasteryl protocatechuate (PRO), stigmasteryl sinapate (SIN) from thermogravimetric analysis.

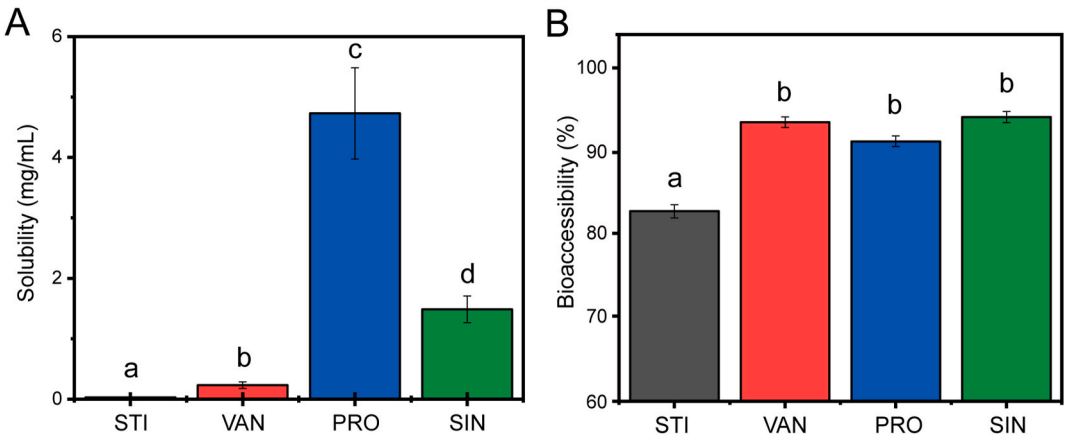

Fig. 5. The solubility and bioaccessibility characteristics of stigmasterol (STI), stigmasteryl vanillate (VAN), stigmasteryl protocatechuate (PRO) and stigmasteryl sinapate (SIN). (A) Solubility indexes of samples; (B) Bioaccessibility of samples at the entire phase of digestion. The data are presented as the means ± SD of three replications. Different characters indicate significant differences between the compared groups ($p < 0.05$).

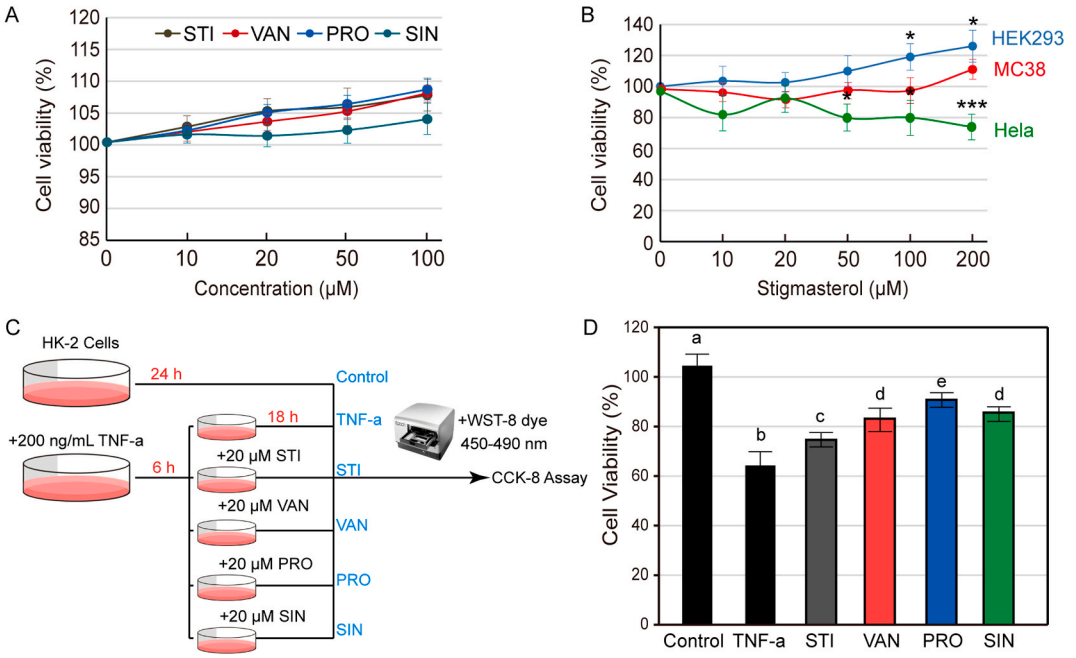

Fig. 6. The assessment of stigmasterol (STI), stigmasteryl vanillate (VAN), stigmasteryl protocatechuate (PRO) and stigmasteryl sinapate (SIN) against the TNF-a induced pro-inflammatory responses in HK-2 cells. (A) The HK-2 cell viability at different concentrations of phytosterol acid esters; (B) The cell viability of HEK293, MC38 and HeLa cell line under the different stigmasterol concentration. "*" indicates a significant difference ($P < 0.05$), and "***" indicates a significant difference ($P < 0.005$) compared with the MC38 model; (C) Schematic depicting approach of the treatment process of the experimental group and the control group followed by measure the absorbance of CCK-8 assay at 450–490 nm; (B) The HK-2 cell viability was determined after treatment. All the data were expressed as a percentage of the control. The data are presented as the means ± SD of five replications. Different characters indicate significant differences between the compared groups ($p < 0.05$).

impact on the viability of different cell lines. As stigmasterol clearly has anti-inflammatory properties (Morgan et al., 2021), here we used 20 μM concentration of phytosterol acid esters, 200 ng/mL TNF-α and HK-2 cells (Huang et al., 2012; Wan et al., 2013) as the treatment and model to evaluate the three new stigmasteryl phenolates (Lee et al., 2017), comparing their anti-inflammatory properties to stigmasterol. The approach was depicted in Fig. 6A. After 24 h treatment of TNF-α, the cell viability was reduced by 36.14%. The 20 μM of STI treatment increased the cell viability by 14.13%. Notably, stigmasteryl phenolates further alleviated the TNF-α induced inflammatory response in this acute renal inflammatory model. Compared to the TNF-α positive and STI groups, the addition of 20 μM VAN, PRO, and SIN for 18 h could significantly reduce the TNF-α induced toxicity, and the cell viability were kept at 82.13%, 88.78% and 83.24%, respectively (Fig. 6B). These results indicate that stigmasterol and phenolic acid have a combined effect in alleviating the TNF-α induced inflammatory response. In HK-2 cells, VAN, PRO and SIN exhibited great anti-inflammatory properties than STI.

3.7. The mitochondrial stress response

Seahorse analyses demonstrated that all stigmasteryl phenolates supplementation increased the basal, maximal OCRs and ATP production in HK-2 cells compared with that of control or STI conditions (Fig. 7A–D). Besides, the PRO showed better mitochondrial respiratory regulation property compared to VAN and SIN at the same dose

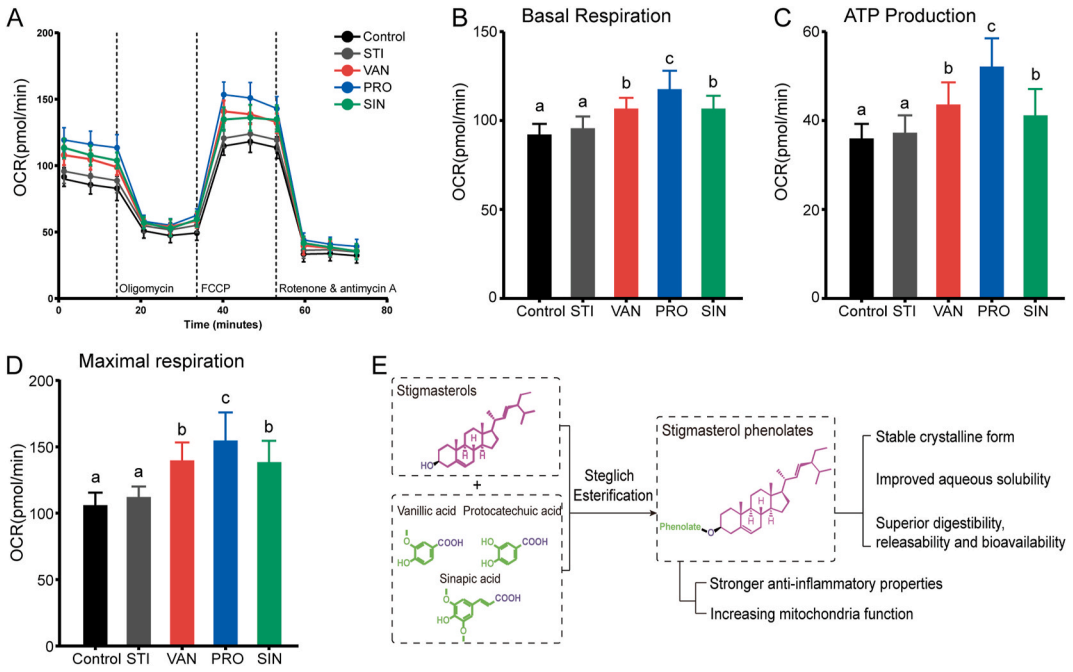

Fig. 7. The assessment of stigmasterol (STI), stigmasteryl vanillate (VAN), stigmasteryl protocatechuate (PRO) and stigmasteryl sinapate (SIN) against the mitochondrial stress test in HK-2 cells. (A) The oxygen consumption rate (OCR) changes of cultured cells after 24h treatment, measured by Seahorse analysis; (B) The basal OCR; (C) The ATP production; (D) The maximal OCR; All the data were expressed as a percentage of the control. The data are presented as the means ± SD of five replications. Different characters indicate significant differences between the compared groups ($p < 0.05$). (E) Diagram of the synthesis, physical and anti-inflammatory properties of the three novel stigmasteryl phenolates. Also, the nutrient-stigmasterol hybrids can be a potential low-toxic and stable targeted mitochondrial delivery strategy.

(Fig. 7A–D). Similar to previous studies, we did not find direct effects or sufficiently significant differences ($p < 0.05$) of phytosterols on mitochondrial function under stress in normal cell culture conditions (Nascimento et al., 2020). Although phytosterols are considered to be resistant to oxidative stress and lipid peroxidation via estrogen receptor mediated PI3K/GSK3 signaling (Shi et al., 2013), and increasing mitochondrial membrane potential under stress conditions (Wong et al., 2016). Interestingly, previous studies highly recommend that phytosterols have a better effect to the mitochondrial function in low glucose-containing medium (Nascimento et al., 2020). Notably, protocatechuic acid (Abdelmageed et al., 2021), sinapic acid (Cherng et al., 2013), and vanillic acid (Chang et al., 2015) are associated with hypoglycemia, which is considered one reason for the improvement of mitochondrial functional regulation by stigmasteryl phenolates. More importantly, incorporation of phytosterols into mitochondrial membrane are believed to enhance mitochondrial function by promoting inner mitochondrial membrane fluidity (Shi et al., 2013; Wong et al., 2016), so that the constructed nutrient-phytosterol conjugates could be a low-toxic and stable targeted mitochondrial delivery strategy to enhance mitochondrial function.

4. Conclusion

Motivated by the known bioactivities of stigmasterols and phenolic acids, we utilized screening experiments to optimize their conjugation. Three stigmasteryl phenolates were prepared: stigmasteryl vanillate (VAN), stigmasteryl protocatechuate (PRO), and stigmasteryl sinapate (SIN), which drive the analysis and preparation of phytosterol organic acid esters in food and make their large-scale application in functional research possible. The chemical structures of these new conjugates were confirmed. The purity of these esters was about 95% by NMR. The diagram of the synthesis, physical, anti-inflammatory and mitochondrial regulation properties of the three stigmasteryl phenolates was shown in Fig. 7E. These results suggest that our synthesized stigmasteryl phenolates improved digestibility and bioaccessibility in terms of physical properties. More interestingly, the nutrient-stigmasterol hybrids tactic we have constructed is practical and can become a targeted mitochondrial delivery strategy with enhanced anti-inflammatory effects, low toxicity, and stability, and is expected to achieve conversion in food additives.

CRediT authorship contribution statement

Xinyue Zou: is one of the co-first authors that contributed equally to this work, performed experiments, Formal analysis, Writing – review & editing. **Ting Xu:** performing experiments, Formal analysis. **Tian Zhao:** Formal analysis. **Jing Xia:** Formal analysis. **Feifan Zhu:** Formal analysis. **Yu Hou:** Formal analysis. **Baiyi Lu:** Formal analysis, Funding acquisition. **Yunfei Zhang:** Conceptualization, Methodology, Writing – review & editing, Funding acquisition, Project administration. **Xuan Yang:** Conceptualization, Methodology, performed experiments, Formal analysis, Writing – review & editing, Funding acquisition, Supervision, Project administration.

Declaration of competing interest

The authors declare that they have no known competing financial interests or personal relationships that could have appeared to influence the work reported in this paper.

Data availability

No data was used for the research described in the article.

Acknowledgement

This work was supported by the Jiangxi Province Major Science and Technology Research and Development Projects (20223AAF02015), the

National Natural Science Foundation of China (22101299), the Natural Science Foundation of Zhejiang Province (LY22C200005) and the Key Technologies Research and Development Program (2021YFC2103801).

Appendix A. Supplementary data

Supplementary data to this article can be found online at https://doi.org/10.1016/j.crfs.2024.100702.

References

Abdelmageed, M.E., Shehatou, G.S.G., Suddek, G.M., Salem, H.A., 2021. Protocatechuic acid improves hepatic insulin resistance and restores vascular oxidative status in type-2 diabetic rats. Environ. Toxicol. Pharmacol. 83, 103577 https://doi.org/10.1016/j.etap.2020.103577.

Amaral, J.S., Casal, S., Pereira, J.A., Seabra, R.M., Oliveira, B.P.P., 2003. Determination of sterol and fatty acid compositions, oxidative stability, and nutritional value of six walnut (Juglans regia L.) cultivars grown in Portugal. J. Agric. Food Chem. 51 (26), 7698–7702. https://doi.org/10.1021/jf030451d.

Andersen, C.J., 2022. Lipid metabolism in inflammation and immune function. Nutrients 14 (7), 1414–1417. https://doi.org/10.3390/nu14071414.

Andreasen, M.F., Landbo, A.-K., Christensen, L.P., Hansen, Å., Meyer, A.S., 2001. Antioxidant effects of phenolic rye (secale cereale L.) extracts, monomeric hydroxycinnamates, and ferulic acid dehydrodimers on human low-density lipoproteins. J. Agric. Food Chem. 49 (8), 4090–4096. https://doi.org/10.1021/jf0101758.

Ashokkumar, N., Vinothiya, K., 2023. Protective impact of vanillic acid on lipid profile and lipid metabolic enzymes in diabetic hypertensive rat model generated by a high-fat diet. Curr. Drug Discov. Technol. 20 (3), 66–73. https://doi.org/10.2174/1570163820666230224100643.

Bao, L., Liu, C., Li, W., Yu, J., Wang, M., Zhang, Y., 2022. Electrochemical synthesis of polysubstituted oxazoles from ketones and acetonitrile. Org. Lett. 24 (31), 5762–5766. https://doi.org/10.1021/acs.orglett.2c02252.

Brodkorb, A., Egger, L., Alminger, M., Alvito, P., Assunção, R., Ballance, S., Recio, I., 2019. INFOGEST static in vitro simulation of gastrointestinal food digestion. Nat. Protoc. 14 (4), 991–1014. https://doi.org/10.1038/s41596-018-0119-1.

Broughton, R., Beaudoin, F., 2021. Analysis of free and esterified sterol content and composition in seeds using GC and ESI-MS/MS. Methods Mol. Biol. 2295, 179–201. https://doi.org/10.1007/978-1-0716-1362-7_11.

Cercaci, L., Rodriguez-Estrada, M.T., Lercker, G., 2003. Solid-phase extraction-thin-layer chromatography-gas chromatography method for the detection of hazelnut oil in olive oils by determination of esterified sterols. J. Chromatogr. A 985 (1–2), 211–220. https://doi.org/10.1016/s0021-9673(02)01397-3.

Chang, W.C., Wu, J.S., Chen, C.W., Kuo, P.L., Chien, H.M., Wang, Y.T., Shen, S.C., 2015. Protective effect of vanillic acid against hyperinsulinemia, hyperglycemia and hyperlipidemia via alleviating hepatic insulin resistance and inflammation in high-fat diet (HFD)-Fed rats. Nutrients 7 (12), 9946–9959. https://doi.org/10.3390/nu7125514.

Cherng, Y.G., Tsai, C.C., Chung, H.H., Lai, Y.W., Kuo, S.C., Cheng, J.T., 2013. Antihyperglycemic action of sinapic acid in diabetic rats. J. Agric. Food Chem. 61 (49), 12053–12059. https://doi.org/10.1021/jf403092b.

Clifton, P.M., Noakes, M., Sullivan, D., Erichsen, N., Ross, D., Annison, G., Nestel, P., 2004. Cholesterol-lowering effects of plant sterol esters differ in milk, yoghurt, bread and cereal. Eur. J. Clin. Nutr. 58 (3), 503–509. https://doi.org/10.1038/sj.ejcn.1601837.

Dhar, A., Lee, K.-S., Dhar, K., Rosazza, J.P.N., 2007. Nocardia sp. vanillic acid decarboxylase. Enzym. Microb. Technol. 41 (3), 271–277. https://doi.org/10.1016/j.enzmictec.2007.02.002.

Di Trani, J.M., Moe, A., Riepl, D., Saura, P., Kaila, V.R.I., Brzezinski, P., Rubinstein, J.L., 2022. Structural basis of mammalian complex IV inhibition by steroids. Proc. Natl. Acad. Sci. USA 119 (30), e2205228119. https://doi.org/10.1073/pnas.2205228119.

Flakelar, C.L., Prenzler, P.D., Luckett, D.J., Howitt, J.A., Doran, G., 2017. A rapid method for the simultaneous quantification of the major tocopherols, carotenoids, free and esterified sterols in canola (Brassica napus) oil using normal phase liquid chromatography. Food Chem. 214, 147–155. https://doi.org/10.1016/j.foodchem.2016.07.059.

Fu, Y., Zhang, Y., Hu, H., Chen, Y., Wang, R., Li, D., Liu, S., 2014. Design and straightforward synthesis of novel galloyl phytosterols with excellent antioxidant activity. Food Chem. 163, 171–177. https://doi.org/10.1016/j.foodchem.2014.04.093.

Gu, Xia, Ma, Yuan, Liu, Yi, Wan, Qiang, 2020 Dec 30. Measurement of mitochondrial respiration in adherent cells by Seahorse XF96 Cell Mito Stress Test. STAR Protoc. 2 (1), 100245 https://doi.org/10.1016/j.xpro.2020.100245.

He, W.-S., Wang, H.-H., Jing, Z.-M., Cui, D.-D., Zhu, J.-Q., Li, Z.-J., Ma, H.-L., 2018. Highly efficient synthesis of hydrophilic phytosterol derivatives catalyzed by ionic liquid. J. Am. Oil Chem. Soc. 95 (1), 89–100. https://doi.org/10.1002/aocs.12024.

Huang, L., Tang, Y., Qin, J., Peng, Y., Yuan, Q., Zhang, F., Tao, L., 2012. Vasoactive intestinal peptide enhances TNF-α-induced IL-6 and IL-8 synthesis in human proximal renal tubular epithelial cells by NF-κB-dependent mechanism. Inflammation 35 (3), 1154–1160. https://doi.org/10.1007/s10753-011-9423-4.

Jia, C., Xia, X., Liu, P., Wang, H., Zhang, J., Zhang, X., 2019. Mild and efficient preparation of phytosteryl amino acid ester hydrochlorides and their emulsifying properties. J. Agric. Food Chem. 67 (6), 1749–1759. https://doi.org/10.1021/acs.jafc.8b07153.

Jie, F., Yang, X., Wu, L., Wang, M., Lu, B., 2022. Linking phytosterols and oxyphytosterols from food to brain health: origins, effects, and underlying mechanisms. Crit. Rev. Food Sci. Nutr. 62 (13), 3613–3630. https://doi.org/10.1080/10408398.2020.1867819.

Juurlink, B.H.J., Azouz, H.J., Aldalati, A.M.Z., AlTinawi, B.M.H., Ganguly, P., 2014. Hydroxybenzoic acid isomers and the cardiovascular system. Nutr. J. 13 (1), 63–69. https://doi.org/10.1186/1475-2891-13-63.

Karakida, F., Ikeya, Y., Tsunakawa, M., Yamaguchi, T., Ikarashi, Y., Takeda, S., Aburada, M., 2007. Cerebral protective and cognition-improving effects of sinapic acid in rodents. Biol. Pharm. Bull. 30 (3), 514–519. https://doi.org/10.1248/bpb.30.514.

Lee, H.H., Cho, Y.I., Kim, S.Y., Yoon, Y.E., Kim, K.S., Hong, S.J., Han, W.K., 2017. TNF-α-induced inflammation stimulates apolipoprotein-A4 via activation of TNFR2 and NF-κB signaling in kidney tubular cells. Sci. Rep. 7 (1), 8856–8864. https://doi.org/10.1038/s41598-017-08785-2.

Li, L.-J., Chao, S., Zhao, S.-X., Lu, J., Zhang, X.-Y., Zhao, Y., Ge, Z.-J., 2023. Protocatechuic acid delays postovulatory oocyte ageing in mouse. Mol. Nutr. Food Res. 67 (4), 2200363 https://doi.org/10.1002/mnfr.202200363.

Liu, W., Xiao, B., Wang, X., Chen, J., Yang, G., 2021. Solvent-free synthesis of phytosterol linoleic acid esters at low temperature. RSC Adv. 11 (18), 10738–10746. https://doi.org/10.1039/d1ra00798j.

Mohan, S., Nair, A., Poornima, M.S., Raghu, K.G., 2023. Vanillic acid mitigates hyperinsulinemia induced ER stress mediated altered calcium homeostasis, MAMs distortion and surplus lipogenesis in HepG2 cells. Chem. Biol. Interact. 375, 110365 https://doi.org/10.1016/j.cbi.2023.110365.

Morgan, L.V., Petry, F., Scatolin, M., de Oliveira, P.V., Alves, B.O., Zilli, G.A.L., Müller, L.G., 2021. Investigation of the anti-inflammatory effects of stigmasterol in mice: insight into its mechanism of action. Behav. Pharmacol. 32 (8), 640–651. https://doi.org/10.1097/fbp.0000000000000658.

Nascimento, E.B.M., Konings, M., Schaart, G., Groen, A.K., Lutjohann, D., van Marken Lichtenbelt, W.D., Plat, J., 2020. In vitro effects of sitosterol and sitostanol on mitochondrial respiration in human brown adipocytes, myotubes and hepatocytes. Eur. J. Nutr. 59 (5), 2039–2045. https://doi.org/10.1007/s00394-019-02052-y.

Niwa, T., Doi, U., Kato, Y., Osawa, T., 1999. Inhibitory mechanism of sinapinic acid against peroxynitrite-mediated tyrosine nitration of protein in vitro. FEBS (Fed. Eur. Biochem. Soc.) Lett. 459 (1), 43–46. https://doi.org/10.1016/S0014-5793(99)01216-8.

Osborn, L.J., Claesen, J., Brown, J.M., 2021. Microbial flavonoid metabolism: a cardiometabolic disease perspective. Annu. Rev. Nutr. 41 (1), 433–454. https://doi.org/10.1146/annurev-nutr-120420-030424.

Rui, X., Wenfang, L., Jing, C., Meng, C., Chengcheng, D., Jiqu, X., Shuang, R., 2017. Neuroprotective effects of phytosterol esters against high cholesterol-induced cognitive deficits in aged rat. Food Funct. 8 (3), 1323–1332. https://doi.org/10.1039/C6FO01656A.

Sakamoto, S., Nakahara, H., Shibata, O., 2013. Miscibility behavior of sphingomyelin with phytosterol derivatives by a Langmuir monolayer approach. J. Oleo Sci. 62 (10), 809–824. https://doi.org/10.5650/jos.62.809.

Schär, A., Liphardt, S., Nyström, L., 2017. Enzymatic synthesis of steryl hydroxycinnamates and their antioxidant activity. Eur. J. Lipid Sci. Technol. 119 (5). ARTN160026710.1002/ejlt.201600267.

Semaming, Y., Kumfu, S., Pannangpetch, P., Chattipakorn, S.C., Chattipakorn, N., 2014. Protocatechuic acid exerts a cardioprotective effect in type 1 diabetic rats. J. Endocrinol. 223 (1), 13–23. https://doi.org/10.1530/joe-14-0273.

Shi, C., Wu, F., Zhu, X.C., Xu, J., 2013. Incorporation of beta-sitosterol into the membrane increases resistance to oxidative stress and lipid peroxidation via estrogen receptor-mediated PI3K/GSK3beta signaling. Biochim. Biophys. Acta 1830 (3), 2538–2544. https://doi.org/10.1016/j.bbagen.2012.12.012.

Tai, K., Liu, F., He, X., Ma, P., Mao, L., Gao, Y., Yuan, F., 2018. The effect of sterol derivatives on properties of soybean and egg yolk lecithin liposomes: stability, structure and membrane characteristics. Food Res. Int. 109, 24–34. https://doi.org/10.1016/j.foodres.2018.04.014.

Tan, Z., Shahidi, F., 2013. Phytosteryl sinapates and vanillates: chemoenzymatic synthesis and antioxidant capacity assessment. Food Chem. 138 (2), 1438–1447. https://doi.org/10.1016/j.foodchem.2012.10.093.

Wan, J., Zhou, X., Cui, J., Zou, Z., Xu, Y., You, D., 2013. Role of complement 3 in TNF-α-induced mesenchymal transition of renal tubular epithelial cells in vitro. Mol. Biotechnol. 54 (1), 92–100. https://doi.org/10.1007/s12033-012-9547-2.

Wang, M., Liu, Y., Zhao, T., Xiao, F., Yang, X., Lu, B., 2021a. Dietary sterols and sterol oxidation products on atherosclerosis: an insight provided by liver proteomic and lipidomic. Mol. Nutr. Food Res. 65 (20), e2100516 https://doi.org/10.1002/mnfr.202100516.

Wang, M., Yang, B., Shao, P., Jie, F., Yang, X., Lu, B., 2021b. Sterols and sterol oxidation products: effect of dietary intake on tissue distribution in ApoE-deficient mice. J. Agric. Food Chem. 69 (40), 11867–11877. https://doi.org/10.1021/acs.jafc.1c03648.

Winkler-Moser, J.K., Hwang, H.-S., Bakota, E.L., Palmquist, D.A., 2015. Synthesis of steryl ferulates with various sterol structures and comparison of their antioxidant activity. Food Chem. 169, 92–101. https://doi.org/10.1016/j.foodchem.2014.07.119.

Winter, A.N., Brenner, M.C., Punessen, N., Snodgrass, M., Byars, C., Arora, Y., Linseman, D.A., 2017. Comparison of the neuroprotective and anti-inflammatory effects of the anthocyanin metabolites, protocatechuic acid and 4-hydroxybenzoic acid. Oxid. Med. Cell. Longev., 6297080 https://doi.org/10.1155/2017/6297080, 2017.

Witkowska, A.M., Waśkiewicz, A., Zujko, M.E., Cicha-Mikołajczyk, A., Mirończuk-Chodakowska, I., Drygas, W., 2022. Dietary plant sterols and phytosterol-enriched margarines and their relationship with cardiovascular disease among polish men and women: the WOBASZ II cross-sectional study. Nutrients 14 (13), 2665–2677. https://doi.org/10.3390/nu14132665.

Wong, H.S., Leong, P.K., Chen, J.H., Leung, H.Y., Chan, W.M., Ko, K.M., 2016. beta-Sitosterol increases mitochondrial electron transport by fluidizing mitochondrial membranes and enhances mitochondrial responsiveness to increasing energy demand by the induction of uncoupling in C2C12 myotubes. J. Funct.Foods 23, 253–260. https://doi.org/10.1016/j.jff.2016.02.045.

Yalameha, B., Nejabati, H.R., Nouri, M., 2023. Cardioprotective potential of vanillic acid. Clin. Exp. Pharmacol. Physiol. 50 (3), 193–204. https://doi.org/10.1111/1440-1681.13736.

Yang, X., Li, Y., Zheng, L., He, X., Luo, Y., Huang, K., Xu, W., 2019. Glucose-regulated protein 75 in foodborne disease models induces renal tubular necrosis. Food Chem. Toxicol. 133, 110720 https://doi.org/10.1016/j.fct.2019.110720.

Yu, J., Liu, T., Sun, W., Zhang, Y., 2023. Electrochemical decarboxylative elimination of carboxylic acids to alkenes. Org. Lett. 25 (43), 7816–7821. https://doi.org/10.1021/acs.orglett.3c02997.

Zhang, Y., Gu, Y., Jiang, J., Cui, X., Cheng, S., Liu, L., Zhou, F., 2022. Stigmasterol attenuates hepatic steatosis in rats by strengthening the intestinal barrier and improving bile acid metabolism. npj Science of Food 6 (1), 38–51. https://doi.org/10.1038/s41538-022-00156-0.

Zheng, M.M., Lu, Y., Huang, F.H., Wang, L., Guo, P.M., Feng, Y.Q., Deng, Q.C., 2013. Lipase immobilization on hyper-cross-linked polymer-coated silica for biocatalytic synthesis of phytosterol esters with controllable fatty acid composition. J. Agric. Food Chem. 61 (1), 231–237. https://doi.org/10.1021/jf3042962.